

Swift-BAT Survey of Galactic Sources: Catalog and Properties of
the populations

R. Voss¹

Max Planck Institut für Extraterrestrische Physik, P.O. Box 1603, 85740, Garching,
Germany

rvoss@mpe.mpg.de

and

M. Ajello

SLAC National Accelerator Laboratory and Kavli Institute for Particle Astrophysics and
Cosmology, 2575 Sand Hill Rd, Menlo Park, CA 94304, USA

Received _____; accepted _____

¹Excellence Cluster Universe, Technische Universität München, Boltzmannstr. 2, D-85748, Garching, Germany

ABSTRACT

We study the populations of X-ray sources in the Milky Way in the 15-55 keV band using a deep survey with the *BAT* instrument aboard the *Swift* observatory. We present the logN-logS distributions of the various source types and we analyze their variability and spectra. For the low-mass X-ray binaries (LMXBs) and the high-mass X-ray binaries (HMXBs) we derive the luminosity functions to a limiting luminosity of $L_X \sim 7 \times 10^{34}$ erg s⁻¹. Our results confirm the previously found flattening of the LMXB luminosity function below a luminosity of $L_X \sim 10^{37}$ erg s⁻¹. The luminosity function of the HMXBs is found to be significantly flatter in the 15-55 keV band than in the 2-10 keV band. From the luminosity functions we estimate the ratios of the hard X-ray luminosity from HMXBs to the star-formation rate, and the LMXB luminosity to the stellar mass. We use these to estimate the X-ray emissivity in the local universe from X-ray binaries and show that it constitutes only a small fraction of the hard X-ray background.

Subject headings: Galaxy: stellar content – X-rays: binaries – X-rays: stars

1. Introduction

Large galaxies typically contains hundreds of bright ($> 10^{36}$ erg s $^{-1}$) X-ray sources, of which the majority are high-mass X-ray binaries (HMXBs) or low-mass X-ray binaries (LMXBs). The possibilities of studying them in external galaxies with *XMM-Newton* and *Chandra* have sparked interest in studying the populations of these sources in galaxies. The Milky Way provides a useful reference for such studies. Besides a considerable population of HMXBs in the Magellanic clouds (e.g. Liu et al. 2005), and the detection of a few individual sources in other nearby galaxies (e.g. Pietsch et al. 2006), the Milky Way is the only galaxy in which it is currently, or in the near future, possible to obtain information on a high fraction of the X-ray binaries from measurements in other wavebands than the X-rays. It is also possible to measure X-ray sources in the Milky Way at much lower luminosities than in external galaxies. The X-ray source populations in the Milky Way can therefore provide us with unique observational constraints.

However, the analysis of the population of X-ray sources in the Galaxy suffer from several problems. The Galaxy has a large angular size and the distances to many of the sources are not known. The population of sources is mixed and from X-rays alone it is not always possible to distinguish a weak nearby source from a more distant bright source. Focusing telescopes have small fields of view and are therefore not suited for such studies. Grimm et al. (2002) used the All-Sky Monitor (ASM) of the RXTE observatory to study the populations of X-ray sources in the 2-10 keV band, and constrained the luminosity functions of X-ray binaries with luminosities $\gtrsim 10^{36}$ erg s $^{-1}$. They found that the differential luminosity function of the HMXBs could be approximated by a single power-law with a slope of $\Gamma \simeq -1.6$, whereas the luminosity function of LMXBs was more complicated with a steep slope at high luminosities and a shallow slope at luminosities below 10^{37} erg s $^{-1}$. With *XMM-Newton* and *Chandra* the investigations were extended to also cover nearby

galaxies. Grimm et al. (2003) found that the luminosity function of HMXBs in a sample of star-forming galaxies showed no evidence of variation, and was consistent with the results from the Milky Way slope of $\Gamma \simeq -1.6$, with a possible cut-off at very high luminosities, a few $\times 10^{40}$ erg s $^{-1}$. Investigations of the LMXB populations in old stellar environments also found results consistent with the Milky Way results, with a steep slope at high luminosities and a shallower slope at lower luminosities (e.g. Kim & Fabbiano 2004; Voss & Gilfanov 2006, 2007; Kim et al. 2009). However, the exact shape remains controversial. Gilfanov (2004) combined results from nearby galaxies with those of the Milky Way and found a power-law slope of $\Gamma \simeq -1.0$ at luminosities below 10^{37} erg s $^{-1}$, and a slope of $\Gamma \simeq -1.8$ above this limit, breaking to an even steeper slope at luminosities above 5×10^{38} erg s $^{-1}$. Kim & Fabbiano (2004) studied a larger sample of galaxies, and confirmed the slope of $\Gamma \simeq -1.8$ at luminosities above a few times 10^{37} erg s $^{-1}$, and while a single power-law fit was acceptable, the fit did improve when a break to a steeper slope at high luminosities was included. Studies of the bulge of M31 and the early type galaxy Centaurus A (Cen A, NGC 5128) showed a clear break at low luminosities $\sim 10^{37}$ erg s $^{-1}$ confirming the low-luminosity slope of $\Gamma \simeq -1.0$ (Voss & Gilfanov 2006, 2007; Voss et al. 2009). While initial studies of the elliptical galaxies NGC 3379 and NGC 4278 (Kim et al. 2006) did not show any evidence of this break, deeper observations indicate some flattening towards low luminosities (Kim et al. 2009). Finally, recent results (Voss & Gilfanov 2007; Woodley et al. 2008; Voss et al. 2009; Kim et al. 2009) show that there is a difference between the luminosity functions of LMXBs in globular clusters and those outside, with a dearth of low-luminosity sources in globular clusters.

The *RXTE ASM*, *Chandra* and *XMM-Newton* observatories are only detecting photons below ~ 10 keV. However, many X-ray binaries emit a significant fraction of their energy in harder X-rays. Incomplete knowledge of the different X-ray states, and the time individual

sources stay in these states, makes it difficult to extrapolate the observations below 10 keV to wider bands. Furthermore these telescopes are biased against objects with high absorbing column densities $> 10^{22}\text{cm}^{-2}$ (see e.g. Figure 3 in Ajello et al. 2009), such as the very absorbed HMXBs recently discovered with *INTEGRAL* (e.g. Walter et al. 2006). The first observatory useful for population studies of the Milky Way in hard X-rays (>10 keV) was *INTEGRAL* with its coded-mask telescopes. This capability was used by Lutovinov et al. (2005) to study the spectra and spatial distribution of the Galactic population of HMXBs. A similar study of the LMXBs, including the luminosity function, was carried out by Revnivtsev et al. (2008), but this study was limited to the bulge LMXBs.

In this paper we extend the study of the populations of Galactic X-ray sources in the hard X-rays, utilizing data obtained by the *Burst Alert Telescope* (BAT; Barthelmy et al. 2005), on board the *Swift* satellite (Gehrels et al. 2004). We follow the approach of Grimm et al. (2003), compiling a catalogue of sources based on previously published identifications. These are then analyzed taking into account the limits of the identification procedures.

2. The BAT X-ray Survey

The *BAT* represents a major improvement in sensitivity for imaging of the hard X-ray sky. BAT is a coded mask, wide field of view, telescope sensitive in the 15–200 keV energy range. BAT’s main purpose is to locate Gamma-Ray Bursts (GRBs). While chasing new GRBs, BAT surveys the hard X-ray sky with an unprecedented sensitivity. Thanks to its wide FOV and its pointing strategy, BAT monitors continuously up to 80% of the sky every day. Therefore the light-curves of all sources are sampled regularly in a manner similar to the *RXTE ASM*. Many X-ray sources are highly variable on a variety of timescales, and therefore regular sampling is important for deriving the average properties of objects,

as opposed to pointed observations that are useful for deriving the physical properties of objects at specific times. Results of the *BAT* survey (Markwardt et al. 2005; Ajello et al. 2008a) show that *BAT* reaches a sensitivity of ~ 1 mCrab in 1 Ms of exposure except near bright sources or very crowded fields, where the high backgrounds can worsen the sensitivity by a factor of ~ 2 . Given its sensitivity and the large exposure already accumulated in the whole sky, *BAT* poses itself as an excellent instrument for studying the Galactic source populations.

2.1. Data Processing

For the analysis presented here, we used all the available *BAT* data taken from January 2005 to March 2007. The chosen energy range for the all-sky analysis is 15–55 keV. The lower limit is dictated by the energy threshold of the detectors. The upper limit was chosen as to avoid the presence of strong background lines which could worsen the overall sensitivity. Data were processed using standard Swift software contained in the HEASOFT 6.3.2 distribution. Data screening was performed according to Ajello et al. (2008a). We recall here the main steps. Data are filtered according to the stability of the pointing, the *BAT* array rate (≤ 18000 Hz), the distance to the South Atlantic Anomaly, the goodness of the fit to the *BAT* array background ($\chi_{red} < 1.5$) and the presence of known sources at the correct position in the FOV. Only those data which fulfill these criteria are used for the analysis. The main difference from Ajello et al. (2008a) is that we integrate over energy in the 15–55 keV band instead that in the 14–170 keV band. The all-sky image is obtained as the weighted average of all the shorter (per-pointing) observations. For this analysis, we consider only the sky region along the Galactic Plane whose absolute Galactic latitude is less than 20° . The average exposure in the Galactic region is 2.6 Ms, being 1.3 Ms and 4.1 Ms the minimum and maximum exposure times respectively. The final image shows

a Gaussian normal noise and we identified source candidates as excesses above the 4.8σ level. Above this threshold, we detected 228 objects. Considering that the all-sky image has a pixel size of 8×8 arcmin for a total of 2.25 million pixels, we expect ~ 1.8 spurious detection above the 4.8σ threshold ($\leq 1\%$ of the total number of excesses).

All the candidates are fit with the BAT point spread function (using the standard BAT tool *batcelldetect*) to derive the best source position. The sources found in this way are all those whose averaged emission is above the sensitivity limit of our survey ($\sim 1 - 2 \times 10^{-11}$ erg $\text{cm}^{-2} \text{s}^{-1}$ in the 15-55 keV band, depending on the local exposure and background) at the position of the source. Fast transients, which are detected in the per-pointing analysis only, are not discussed here and their study will be left to a future publication.

2.2. Source Identification

We used high-energy catalogs in order to identify BAT sources. Identification was in most cases a straightforward process, since the cross-correlation of BAT objects with the ROSAT All-Sky Survey Bright Source Catalogue (Voges et al. 1999) provides an easy and solid way to identify a large fraction ($\sim 70\%$) of them (Ajello et al. 2008a). Most of the uncorrelated sources are not present in the ROSAT survey because of absorption (either along the line of sight or intrinsic to the source). However, given the very large exposure INTEGRAL accumulated along the Galactic plane, most of the remaining sources were identified using the Third IBIS Catalog (Bird et al. 2007) and the INTEGRAL all-sky catalog (Krivonos et al. 2007).

We report in Fig. 1, the offset of the BAT sources from the catalogued counterpart as a function of S/N. We determine that the mean offset varies with significance according to

$$\text{OFFSET} = (6.1 \pm 1.5) \times (S/N)^{-0.56(\pm 0.20)} + 0.13 \quad (\text{arcmin}), \quad (1)$$

where the constant of $0.13'$ is due to a systematic misalignment of the boresight which causes the systematic offset of the brightest sources (see also Tueller et al. 2010). At the detection threshold of 4.8σ the average offset is $\sim 2.6'$. Moreover, Fig. 1 shows the standard deviation of the data for different logarithmic bins of source significance. This is found to be always less than $2.5'$. Moreover, Figure 2 shows the difference in the celestial coordinates between the position of the BAT sources and the position of the optical counterpart. In both directions (e.g. right ascension and declination) the distributions are centered in zero and exhibit a similar standard deviation of $1.5'$. All these results confirm the good position accuracy of BAT even in crowded regions as the Galactic plane.

3. Catalog

In Table 1 we report the coordinates, fluxes and other details of the 228 detected sources. Most of the objects have both an identification in other X-ray band and in the optical. In a few cases, the optical classification is still uncertain or unknown. Only in 5 cases we do not have a secure identification for the BAT object, and 12 further sources do have counterparts, but have unidentified object types. For 4 of the 5 sources without identification we have listed tentative IDs in Table 2. The fluxes quoted in Table 1 are time-averaged fluxes over the whole data set in the 15–55 keV energy band. Conversion from count rate to flux was performed adopting a Crab Nebula spectrum of the form $dN/dE = 10.17 E^{-2.15}$. Position uncertainty for the BAT objects can be derived, as a function of significance, using Equation 1. We derive that the average location accuracy for a 5, 10 and 20σ source is $2.6'$, $1.8'$ and $1.2'$. For comparison, the location accuracies reported for INTEGRAL-IBIS for the same significances are $2.1'$, $1.5'$ and $0.8'$ respectively (Krivonos et al. 2007). The better location accuracy of INTEGRAL-IBIS is not surprising in view of the fact that the IBIS point spread function is sharper than the BAT one ($12'$

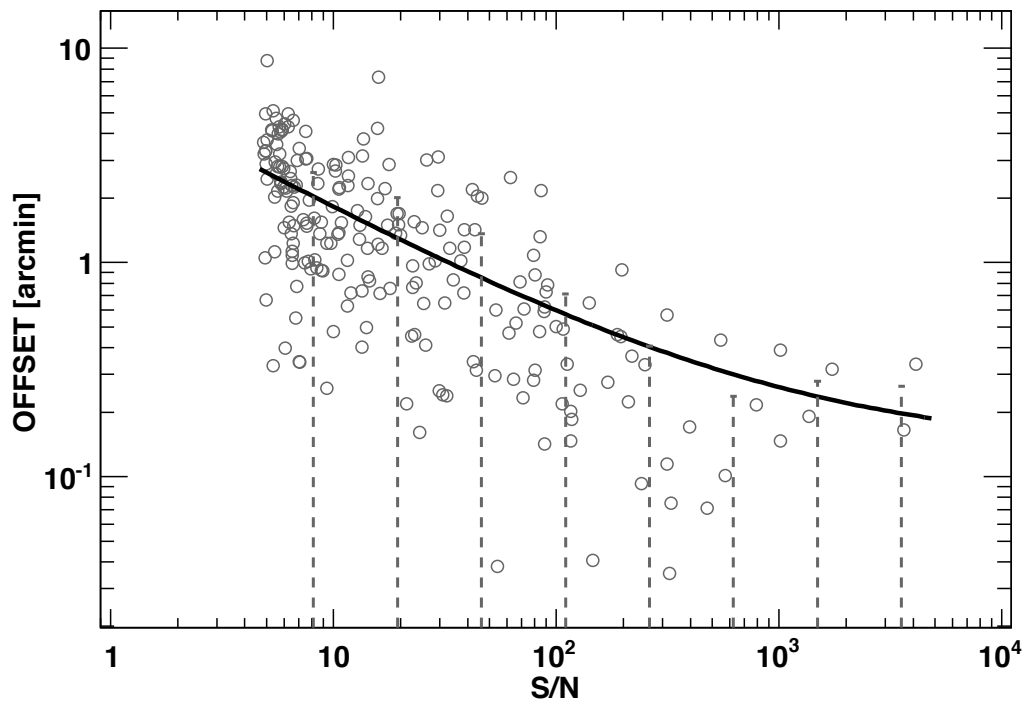


Fig. 1.— Offset from catalog position for the sources reported in Table 1 as a function of S/N (open circles). The solid line represents the best fit to the data (see Eq. 1) and gives the mean offset vs. S/N. The dashed lines show the standard deviation of the offset distribution in several bins of S/N.

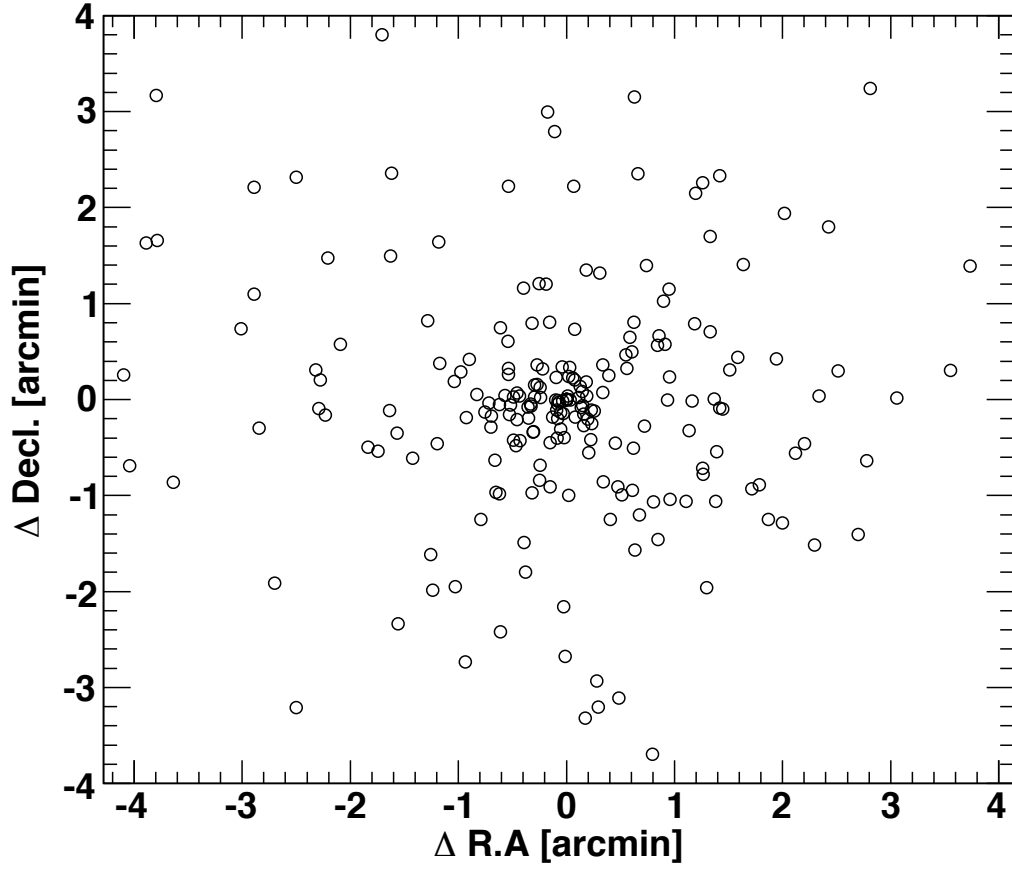


Fig. 2.— Difference in right ascension and declination between the positions of the BAT sources and the position of their optical counterparts.

versus $22'$ full width at half maximum, see Bird et al. 2006; Barthelmy et al. 2005).

Many of the X-ray binaries have known distances, albeit with large uncertainties, and the catalogue includes the approximate distances to HMXBs taken from Liu et al. (2006) and to LMXBs from Liu et al. (2007). In Table 3 we give the numbers of different identified source types, and in Figure 3 the distribution of the source types on the sky is shown.

Figure 4 shows the inner $20^\circ \times 10^\circ$ region around the Galactic center where BAT detects more than 30 sources. Particularly, when looking at the Galactic center, the similarity of the BAT and the INTEGRAL images is apparent (Revnivtsev et al. 2004; Bird et al. 2006) although BAT is unable to resolve all the sources in this complex region. Two of the sources reported in the map are not part of this work because their significance, when integrated over the 2 years of the survey, is lower than 4.8σ . Indeed, they are transient sources which are detected by BAT only during their outburst episodes. One source is XTE J1747-274 which is a neutron star LMXB which was very active particularly in March-April 2005 (see e.g. Zhang et al. 2009, and references therein). The other source, IGR J17391-3021, is a supergiant fast X-ray transient characterized by very short intense bursts lasting on the order of hours (e.g. Smith et al. 2006). This source was particularly active in BAT during 2006.

4. Spectral Properties

For each object in our survey we extracted a 15–195 keV spectrum with the method described in Ajello et al. (2008c). Here we recall the main steps: for a given source, we extract a spectrum from each observation where the source is in the field of view. These spectra are corrected for residual background contamination and for vignetting; the per-pointing spectra are then (weighted) averaged to produce the final source spectrum. Thus, the final spectrum represents the average source emission over the time-span

considered here. The accuracy of these spectra is discussed in details in Ajello et al. (2009).

The average spectral properties of the sample can be studied by means of hardness ratios (HR) which are defined as normalized differences between the background-subtracted count-rates in the soft band (S, 14–22 keV), in the medium band (M, 22–50 keV) and in the hard band (H, 50–195 keV).

These HRs are defined respectively as:

$$HR_1 = \frac{M - H}{M + H}, \quad HR_2 = \frac{S - H}{S + H}, \quad (2)$$

The hardness ratios, shown in Fig. 5, are normalized to the range -1 and +1 setting negative count-rates to zero.¹ However, as a test we allowed negative count-rates to exist and we found that only 3 objects have an hardness ratio value which falls outside the above range. All these objects are LMXBs with basically no detection in the hard-band. Thus, the results reported below do not change whether negative count-rates are set to zero or not. In this plot, hard power-law sources (e.g. AGNs) occupy the central part of the diagram while soft sources tend to move to positive values of HR_1 . All the detected sources reported in Tab. 1 are also shown in Fig. 5 (i.e. no sources have been excluded from the graph) and this is due to the fact that BAT is able to constrain efficiently the source spectrum even in the hard band (50–195 keV). While it is noticeable that all Galactic sources are generally softer than AGNs, a striking feature is the clustering of 20 LMXBs at large values of both HR_1 and HR_2 . The combination of the two points to the fact that these sources exhibit an extremely soft spectrum below 50 keV and an hard spectrum above this energy. To investigate this

¹As shown in Ajello et al. (2009), the analysis of off-source positions showed that, in each energy channel, the count-rates are found consistent with zero within errors. Thus, a few negative count-rates consistent with zero (particularly at high energy) can be interpreted as a non-detection of the source in that band.

more in details we created a stacked spectrum of LMXBs with $HR_2 > 0.6$ and < 0.6 . These are shown in Fig. 6 along with the best-fit models. Indeed LMXBs clustering in the upper-right corner of the HR plot exhibit a spectrum which is dominated by a bright black body component ($kT=2.70\pm 0.70$ keV) at low energy and by a flat power law (index of 1.6 ± 0.4) at high energy. This corresponds to the high/soft state typical of bright LMXBs. On the other hand, all the other LMXBs are characterized by a power-law type spectrum with a photon index of 2.74 ± 0.06 , corresponding to the low/hard state. The analysis of the stacked spectra of all Galactic source classes (with more than 5 objects) is reported in Table 4. From this analysis it is evident that most Galactic sources have a non-negligible hard X-ray emission which extends all the way up to 200 keV and that can be modeled as a power law. The only exception is represented by the CV class whose average spectrum is softer than a power law and consistent with a bremsstrahlung model with a temperature of ~ 22 keV (see e.g. Brunschweiler et al. 2009).

The stacked spectrum of all the CVs (19) detected by BAT is reported in Fig. 7.

5. Variability Analysis

To estimate the variability of the sources in our catalogue, we find numerical maximum-likelihood estimates of the intrinsic variability (Almaini et al. 2000) which has for example been used in the analysis of AGN from *XMM-Newton* (Mateos et al. 2007) and *Swift/BAT* (Beckmann et al. 2007) observations. In this method, the intrinsic variability σ_Q is found from solving

$$\sum_{i=0}^N \frac{(x_i - \bar{x})^2 - (\sigma_i^2 + \sigma_Q^2)}{(\sigma_i^2 + \sigma_Q^2)^2} = 0, \quad (3)$$

where x_i and σ_i are the measured count rate and error in each time bin i . As in Beckmann et al. (2007), we applied this method to the light curves with different time binnings of 1, 7,

20 and 40 days, and use the variability relative to the average count rate σ_Q/\bar{x} to estimate the strength of the variability. We simulated random light curves based on the observed source fluxes and errors. These were used to obtain Monte Carlo estimates of the errors on the calculated variabilities. We use both lightcurves generated at random positions and objects that are expected to be constant (supernova remnants) to investigate systematical effects caused by the instruments or the data analysis. For the random positions, we find an average variability of $\sigma_Q=6.0 \times 10^{-5}$, 1.1×10^{-5} , 4.5×10^{-6} and $2.5 \times 10^{-6} \text{ s}^{-1}$ for 1, 7, 20 and 40 days time binnings, respectively. From the supernova remnants, the systematic variability is seen to increase with increasing count rate, up to $\sigma_Q=1.4 \times 10^{-3}$, 9.7×10^{-4} , 9.0×10^{-4} and $5.9 \times 10^{-4} \text{ s}^{-1}$ for the Crab Nebula. To account for this, we subtracted the variability found at the random positions from the intrinsic variability of our sources. For the bright sources with count rates above 10^{-4} s^{-1} , we furthermore increased the error on the intrinsic variability, by $\sigma_{Crab} \times (\bar{x} - 1.0 \times 10^{-4} \text{ s}^{-1})$. In Fig. 8 we show the intrinsic fractional (σ_Q/\bar{x}) variability of the sources, as a function of the observed count rate, for the 7 day time binning. It is clear that almost all of the strongly variable objects belong to the Galaxy, and the vast majority of these are either HMXBs or LMXBs. Due to their soft spectra, only few stars and CVs are detected in the hard X-rays, and despite extra-Galactic sources being the most numerous source class, they are almost entirely absent from the plot, as only a very small fraction of them are variable above the 10% level (Beckmann et al. 2007). Hard X-ray observations therefore have the potential to classify unidentified X-ray sources. For the sources with known distances, the luminosities can be derived. We caution that deriving distances to Galactic sources is inherently very uncertain and assumption-dependent. Only the bright globular cluster sources and a few very well studied binaries and SNR have distances known to a precision better than 10-20%, whereas the distances to some of the fainter sources can be uncertain by a factor of $\gtrsim 2$. We do not take the errors into account in our analysis. To significantly impact our conclusions, large

systematical shifts (factor $\gtrsim 5$) of a high fraction of the sources would be necessary, which is unlikely. For the sources with calculated luminosities, we plot the variability as a function of source luminosity in Fig. 9. There is no obvious correlation between the luminosity and the strength of the variability (in the 1-40 days range). Note that the sensitivity decreases towards lower fluxes (but depends strongly on the specific observation pattern). This is the reason that the lower left parts of Fig. 8 and 9 are sparsely populated.

6. Source flux distributions

We use the average fluxes to calculate the source flux distributions for the different object types. The resulting logN-logS relations are shown in Figure 10. The sensitivity of the survey varies with direction and the sky coverage of our survey is shown in Figure 11. We have not corrected the logN-logS for the sky coverage, as such a correction depends on the expected spatial source distribution (see section 7 below for LMXBs and HMXBs). The lack of sources at low flux is therefore obviously caused by the strongly decreasing sky coverage below $\sim 2 \times 10^{-11}$ erg s $^{-1}$ cm $^{-2}$. It is clear that at high fluxes the two most important contributions are the HMXBs and the LMXBs, with the only exception being the Crab Nebula, which is the object with the highest flux in our sample. The third most important object type is the extra-Galactic sources, the contribution of which becomes important at fluxes below 10^{-10} erg s $^{-1}$ cm $^{-2}$. We note that limiting our survey to the Galactic plane strongly limits the importance of the extra-Galactic sources. Comparing Figure 10 to Figure 4 of Grimm et al. (2002), it can be seen that the relative importance of the HMXBs and the LMXBs is different in our 15-55 keV band to their results from the 2-10 keV band. In the hard X-rays, the HMXBs dominate the highest fluxes, with the LMXBs being more important at fluxes below 10^{-9} erg s $^{-1}$, whereas the LMXBs are always dominant in the soft X-rays. This is due to the fact that the luminous LMXBs have very

soft spectra, and therefore emit almost negligible amounts of hard X-rays. For example Revnivtsev et al. (2008) found the typical ratio of hard (17-60 keV) to soft (2-10 keV) luminosities to be ~ 30 times lower for LMXBs with luminosities above 2×10^{37} erg s $^{-1}$ than for fainter LMXBs. A similar spectral break is not seen for the HMXBs.

7. Luminosity functions of X-ray binaries

For the majority of bright X-ray binaries in the Galaxy the distances are known within a factor of 2-3 (see discussion above). It is therefore possible to calculate the luminosity functions of the X-ray binaries. The other types of objects studied in this paper do not have adequate numbers of determined distances.

The sensitivity of the survey varies with the direction and the luminosity of the X-ray sources. Following Grimm et al. (2002) we account for this by setting up a model for the Galaxy and for the range of luminosities investigated we estimate the fraction of the Galaxy that is visible. As in Grimm et al. (2002), we use the three-component model of Bahcall & Soneira (1980) for the spatial distribution of the LMXBs, consisting of a disk, a bulge and spheroid. The parameters were chosen to fit the observed distribution of LMXBs (see equations 4–6 and Table 4 of Grimm et al. 2002), and the disk:bulge:spheroid mass ratios were chosen to be 2:1:0.8, where the mass of the spheroid is enhanced to account for the LMXBs formed in globular clusters. As the HMXBs are associated with the young stellar population in the Galaxy, only the disk component is considered relevant for the spatial distribution. To account for the spiral structure of the Galaxy, a spiral model based on optical and radio observations of giant HII regions (Georgelin & Georgelin 1976; Taylor & Cordes 1993) was assumed. This model consists of 4 spiral arms, which were assumed to have Gaussian density profiles along the Galactic plane, with a width of 600 pc. The disk model was modulated by the spiral pattern: 20% for the LMXBs and 100% for the HMXBs.

For all directions we used the local background to estimate the limiting flux detectable by our survey, and used this to create a sensitivity map. For a given X-ray luminosity and direction, this enabled us to calculate the maximum distance, for which a X-ray binary is observable. However, to identify an X-ray source as an X-ray binary, and to determine the distance, it is necessary to have an optically identified counterpart. Grimm et al. (2002) estimated that above a distance of 10 kpc from the sun, the optical identification of X-ray binaries becomes incomplete. We adopt this result and limit our survey to this distance, irrespective of the X-ray brightness of the X-ray binaries. However towards the galactic bulge, source confusion and extinction are serious and optical/IR identifications are incomplete beyond $\sim 2 - 3$ kpc.

Combining the X-ray and optical limits with the model of the Galaxy, we estimate the fraction of the Galaxy observable as a function of source luminosity. This is shown in Fig. 12. Due to our distance constraints and sky coverage, even the brightest sources are limited to a part of the galaxy, and for this reason the lines do not reach a value of one. The total Galactic luminosity functions of LMXBs and HMXBs are now found by correcting the observed luminosity functions for the fraction of the Galaxy probed by our survey. The outcome is shown for the LMXBs in Fig. 13 and the HMXBs in Fig. 14. Also shown in these figures are the luminosity functions obtained if the inner 10 deg of the bulge are excluded from our analysis, to assess the effects of source confusion. Obviously the luminosity function of the HMXBs is not affected, as these are not concentrated in the bulge. On the other hand, the luminosity function of the LMXBs is somewhat different with a lower normalization around 10^{36} erg s $^{-1}$. At both lower and higher luminosities the results are in agreement with the sample including the inner bulge. This is somewhat surprising as incompleteness due to a lack of optical IDs is expected to lead to the opposite effect, and

could indicate a higher normalization of LMXBs per unit stellar mass in the bulge than in the disk. However, the statistical uncertainties, together with the uncertainties of distance determination and the mass distribution of the Galaxy (both of which are difficult to quantify), are too large for such a conclusion to be significant. We note that recent results (Kim & Fabbiano 2010) indicate that the LMXB luminosity functions are age dependent at bright end ($> 10^{38}$ erg s $^{-1}$).

We use Maximum Likelihood (ML) fitting of broken power-laws to analyze the shape of the luminosity functions (using the full samples including the bulge). The resulting ranges and slopes are shown in Table 5. The faint slope of the LMXBs is slightly flatter than, but consistent with $\Gamma=1$, which is consistent with the INTEGRAL observations of the LMXBs in the Galactic bulge (Revnivtsev et al. 2008), and with the soft X-ray results of Gilfanov (2004); Voss & Gilfanov (2006, 2007). Due to the strong spectral change at luminosities of $\sim 10^{37}$ erg s $^{-1}$ (Revnivtsev et al. 2008), the LMXB luminosity function breaks and becomes very steep at higher luminosities. The HMXB fit gives a faint slope of $\gamma = -1.3_{-0.2}^{+0.3}$ for the HMXBs. This is somewhat shallower, but consistent with the ~ -1.6 slope found in the soft band both in the Milky Way (Grimm et al. 2002) and in other galaxies (Grimm et al. 2003). There is a clear break at luminosities above $\sim 2 \times 10^{37}$ erg s $^{-1}$, which is different from the single power-law shape seen in the soft X-rays. We note that the results are not strongly dependent on the few brightest sources. If the two brightest LMXB and HMXB sources are removed from our samples and the fits are repeated, the best-fit parameters are within the quoted errors.

7.1. Total luminosity

We find the combined luminosity from the Milky Way from summing all the sources with the individual incompleteness factors. This gives a hard X-ray luminosity of

$1.3 \pm 0.6 \times 10^{38}$ erg s⁻¹ for the HMXBs and $1.7 \pm 0.4 \times 10^{38}$ erg s⁻¹ for the LMXBs. We note that the total emission is very dependent on the few brightest X-ray binaries (Gilfanov et al. 2004). The total luminosity can also be found by integrating the broken power-law fits to the observed sources, which gives $1.4_{-0.3}^{+1.5} \times 10^{38}$ erg s⁻¹ for the HMXBs and $1.5_{-0.3}^{+1.5} \times 10^{38}$ erg s⁻¹ for the LMXBs. For comparison, the luminosities in the soft band were found to be 2.0×10^{38} erg s⁻¹ for the HMXBs and 2.5×10^{39} erg s⁻¹ for the LMXBs (Grimm et al. 2002). As the HMXBs have a relatively hard spectrum, the total luminosity in the 15-55 keV band is comparable to the soft luminosity, whereas the soft spectra of the brightest LMXBs causes their total hard band luminosity to be only 10% of the soft band luminosity. We note that, as above, the results from removing the brightest sources are within the quoted errors.

The number of HMXBs is roughly proportional to the star-formation rate of a galaxy (Grimm et al. 2003), whereas the LMXBs are related to the stellar mass of their host galaxy (Gilfanov 2004). The total luminosities should therefore be compared to the star-formation rate in the Milky Way estimated to be $2-4M_{\odot}$ yr⁻¹ (Diehl et al. 2006) and the stellar mass of $4.8 - 5.5 \times 10^{10} M_{\odot}$ (Flynn et al. 2006). From this we obtain the ratios: $L_x(HMXB)/\text{SFR} \sim 3 - 7 \times 10^{37}$ erg s⁻¹ M_{\odot}^{-1} yr and $L_x(LMXB)/M_{\text{stellar}} \sim 3 - 6 \times 10^{27}$ erg s⁻¹ M_{\odot}^{-1} .

A part of the diffuse X-ray background comes from X-ray sources in galaxies, and our results can be used to calculate the importance. The local stellar density is $M_* \sim 5 \times 10^8 M_{\odot} \text{Mpc}^{-3}$ (Salucci & Persic 1999; Cole et al. 2001), and the local star-formation rate is $\dot{\rho}_* = 0.015 M_{\odot} \text{Mpc}^{-3} \text{yr}^{-1}$ (Hanish et al. 2006). This gives a local emissivity from X-ray binaries of $\sim 2 - 4 \times 10^{36}$ erg s⁻¹ Mpc⁻³, with approximately 80% coming from the LMXBs. This can be converted to incident flux I_{XRB} using equation 19 of Barcons et al. (1995). Assuming a normal galaxy density evolution of $(1+z)^3$, we find a

flux of $1.5 - 3 \times 10^{-11} \text{ erg s}^{-1} \text{ cm}^{-2} \text{ Str}^{-1}$. We therefore conclude that the contribution to the hard X-ray background, which is $9.09 \times 10^{-8} \text{ erg cm}^{-2} \text{ s}^{-1} \text{ sr}^{-1}$ (Ajello et al. 2008b), is negligible.

It should be noted that because of small-number statistics, the total X-ray luminosity of the HMXBs in a galaxy does not scale linearly with the star-formation rate (Grimm et al. 2003), except for galaxies with very high star-formation rates. The Milky Way might therefore provide a significant under-estimation of the actual L_x/SFR ratio. Indeed Grimm et al. (2002) found a ratio of $\sim 5 \times 10^{37} \text{ erg s}^{-1} M_{\odot}^{-1} \text{ yr}$, similar to our results, whereas Grimm et al. (2003) find an average ratio of $2 \times 10^{39} \text{ erg s}^{-1} M_{\odot}^{-1} \text{ yr}$ for a large sample of galaxies². However, including this effect still limits the contribution to the X-ray background to $\lesssim 2\%$.

In the soft band galaxies have been found to contribute with $\sim 6 - 12\%$ of the X-ray background (e.g. Ranalli et al. 2005). This is a simple effect of the fact that the X-ray background is quite hard and so the X-ray binaries are on average softer. Furthermore in the hard band there is no contribution from the relatively soft X-rays from diffuse gas (e.g. Bogdán & Gilfanov 2008).

8. Discussion

Our analysis of the Galaxy in hard X-rays with the *Swift* *BAT* instrument shows that the most important sources are HMXBs and LMXBs, after which extra-Galactic sources start to dominate the observations. Compared to the Galaxy in softer X-rays,

²This value is different from the one listed in their paper. Shtykovskiy & Gilfanov (2005) discussed their star formation estimates and found that they corresponded to $\sim 1/3$ of the total star formation rate in the $0.1 - 100 M_{\odot}$ range.

the contribution to the total luminosity from HMXBs is much higher, being $\sim 40\%$ in our observations, compared to $\lesssim 10\%$ in the 2-10 keV band (Grimm et al. 2002). This is mainly due to the fact that luminous LMXBs have very soft spectra, with only a few percent of the X-rays being hard. Soft X-rays from HMXBs have been found to be a good indicator of the star-formation rate in late-type galaxies (Grimm et al. 2003). Our observations show that hard X-rays can potentially be more useful for this purpose, especially in galaxies with mixed populations, due to the lower importance of LMXBs. Also in the hard band, possible contributions from hot X-ray emitting gas are avoided. We note that for nearby galaxies, where the brightest individual sources might be observed with future hard X-ray telescopes, the *number* of HMXBs provide a more reliable estimate of the star formation rate than the total luminosity. Extra-Galactic observations can be compared to our Milky Way estimates by integrating the luminosity function given in Table 5 down to the observational luminosity limit of the observed galaxy. At low luminosities, the background AGNs begin to dominate. It is therefore impossible to infer properties of the populations of weaker sources, if optical counterparts have not been observed. This will only be possible with instruments with much better spatial resolution, where individual parts of the Galaxy can be studied in detail.

9. Conclusions

We have performed the first survey of the entire Galactic plane in X-rays, using the *Swift* *BAT* instrument in the 15-55 keV energy range. Out of the total 228 sources we identified the type of 211. The two most important contributions are the HMXBs and the LMXBs, both of which are also among the most variable objects in the Galaxy. The luminosity function of LMXBs is shown to be consistent with determinations from soft X-rays, and with previously results from a smaller sample observed with INTEGRAL.

On the other hand, the slope of the luminosity function of HMXBs is more shallow than expected. Integrating the total luminosity of the X-ray binaries and extra-polating to other galaxies, we find that unresolved populations in galaxies contribute with a relatively small amount to the hard X-ray background.

This research has made use of data obtained from the High Energy Astrophysics Science Archive Research Center (HEASARC) provided by NASA’s Goddard Space Flight Center, of the SIMBAD Astronomical Database which is operated by the Centre de Données astronomiques de Strasbourg, and of the ROSAT All Sky Survey maintained by the Max Planck Institut für Extraterrestrische Physik.

Facilities: Swift (BAT/XRT) .

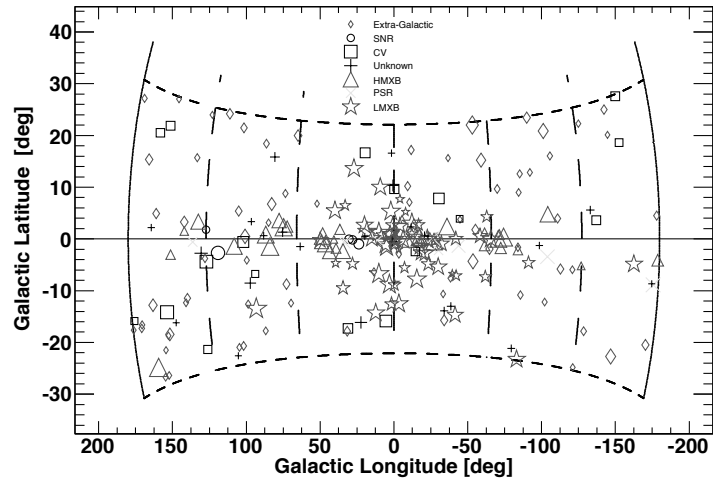


Fig. 3.— AITOFF projection of the distribution of sources on the sky, divided by source type. The size of the symbols is proportional to the source flux.

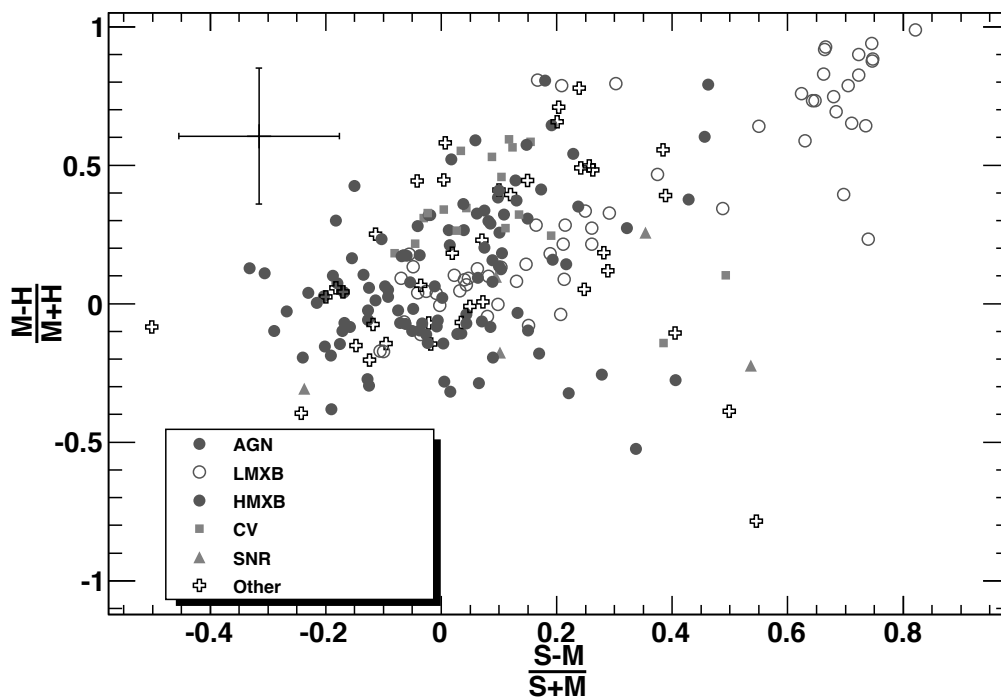


Fig. 5.— Hardness ratio plot of the BAT Galactic sample. In the upper left corner the typical $\pm 1\sigma$ error for a 5σ source is shown.

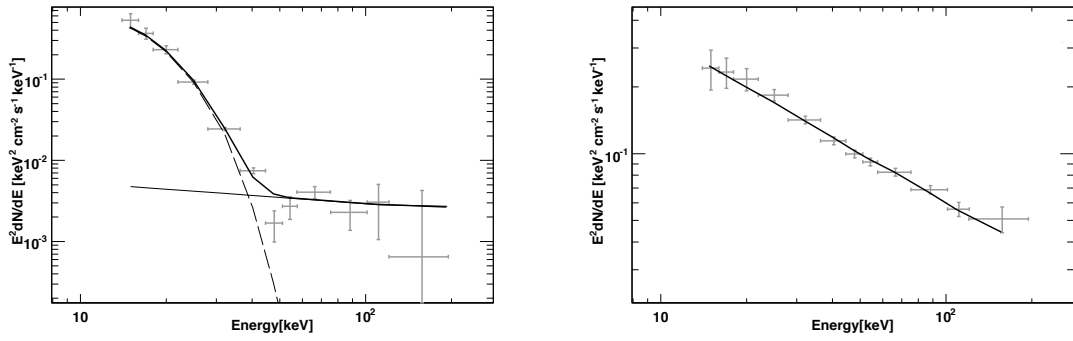


Fig. 6.— Average spectra of LMXB with $HR_2 > 0.6$ (left) and < 0.6 (right) respectively (see § 4 for a definition of the hardness ratio HR_2). The solid lines are the best fit models (power law plus black body for left and power law for right.)

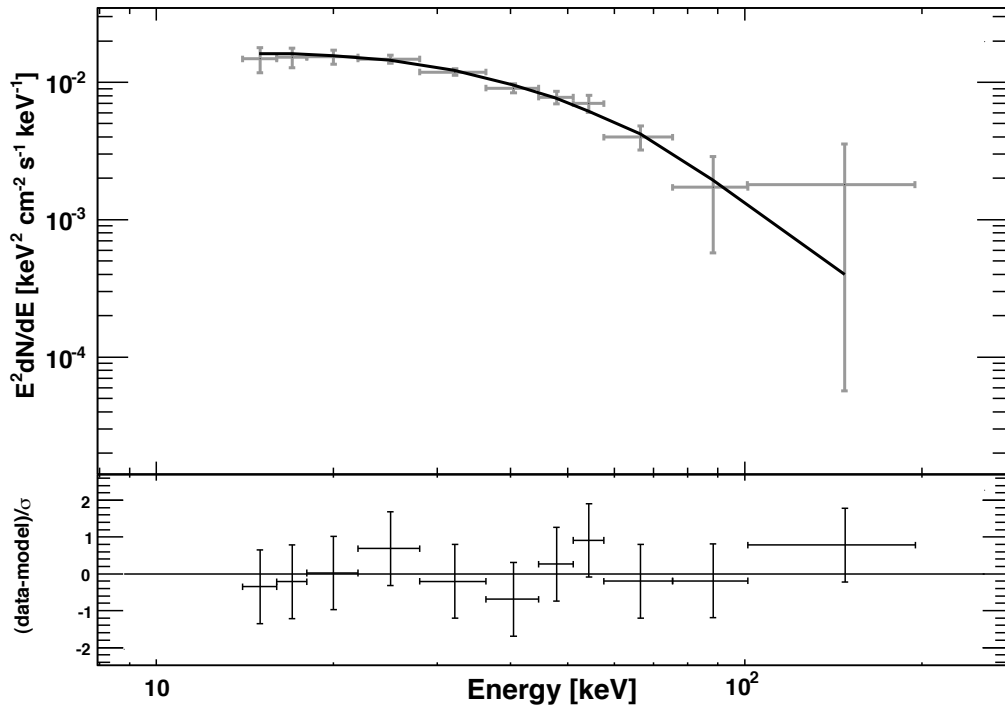


Fig. 7.— Stacked spectrum of the CVs detected by BAT. The solid line represent the best fit to the data (e.g. a bremsstrahlung model with a temperature of $22.68^{+2.39}_{-2.08}$ keV.)

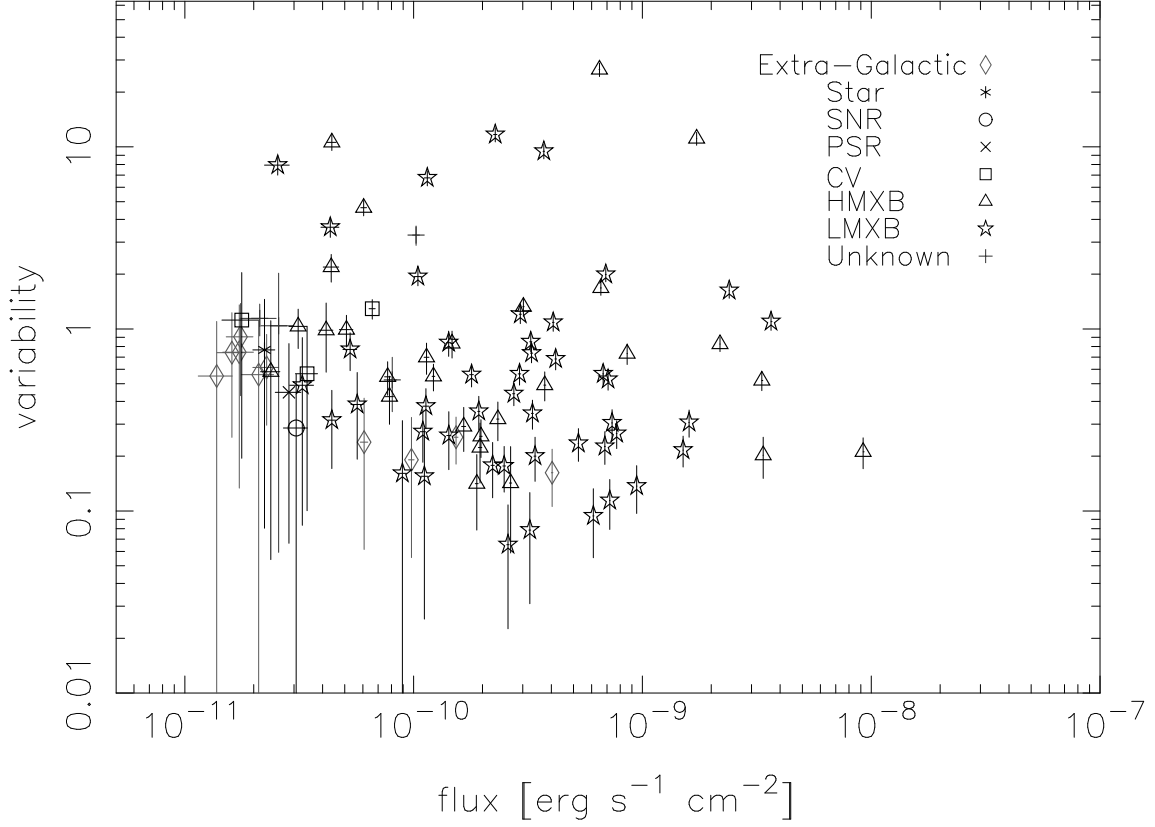


Fig. 8.— Intrinsic fractional variability (σ_Q/\bar{x}) of the sources, as a function of the observed count rate, for the 7 day time binning. Only objects with a variability greater than 2σ are included. For low count rates even sources with high variability are rejected by this criterion, and for this reason the lower left corner of the Figure is sparsely populated. The source types are defined in the catalogue, except for: Extra-Galactic, which is combined of the Seyfert, Blazar, Galaxy and Galaxy cluster types; Star, which covers Symbiotic stars, Be stars and a dwarf nova; Unknown, which are all objects not identified as any of the given types.

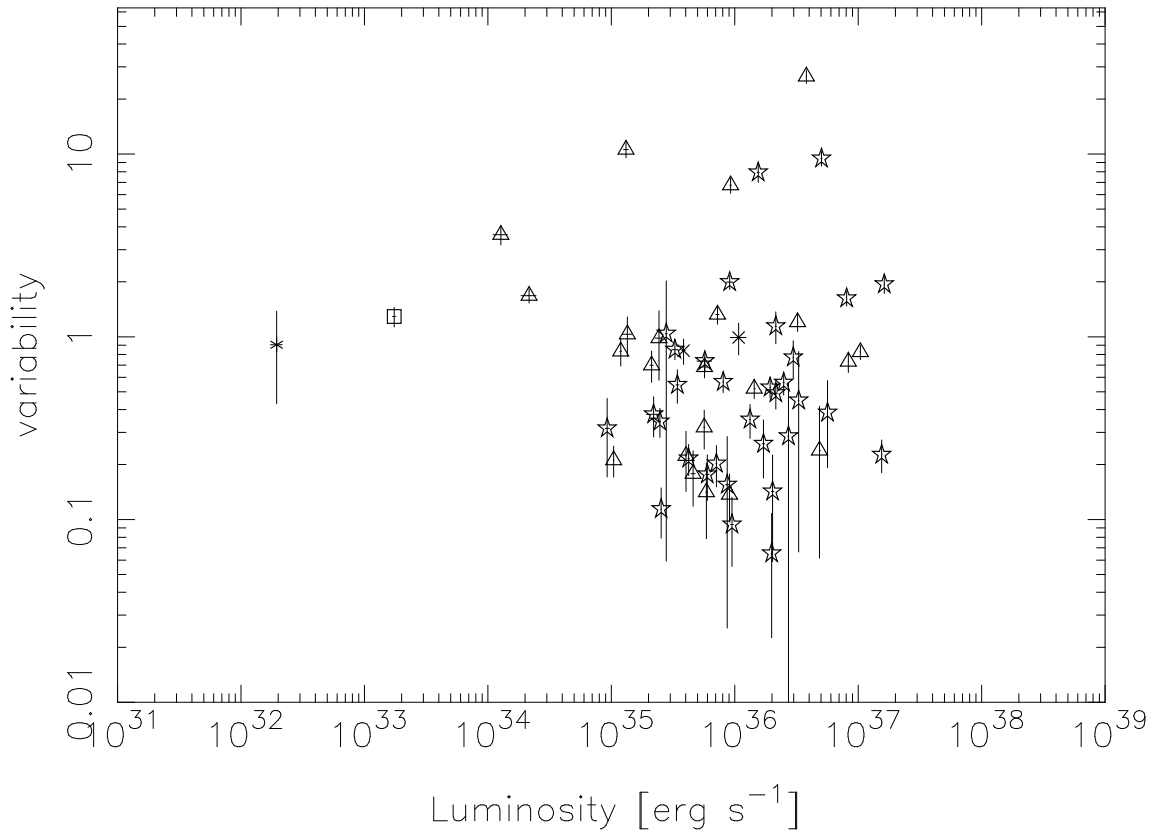


Fig. 9.— Intrinsic variability (σ_Q) of the sources, as a function of the observed luminosity, for the 7 day binning. Only objects with a variability greater than 2σ and with known distances are included.

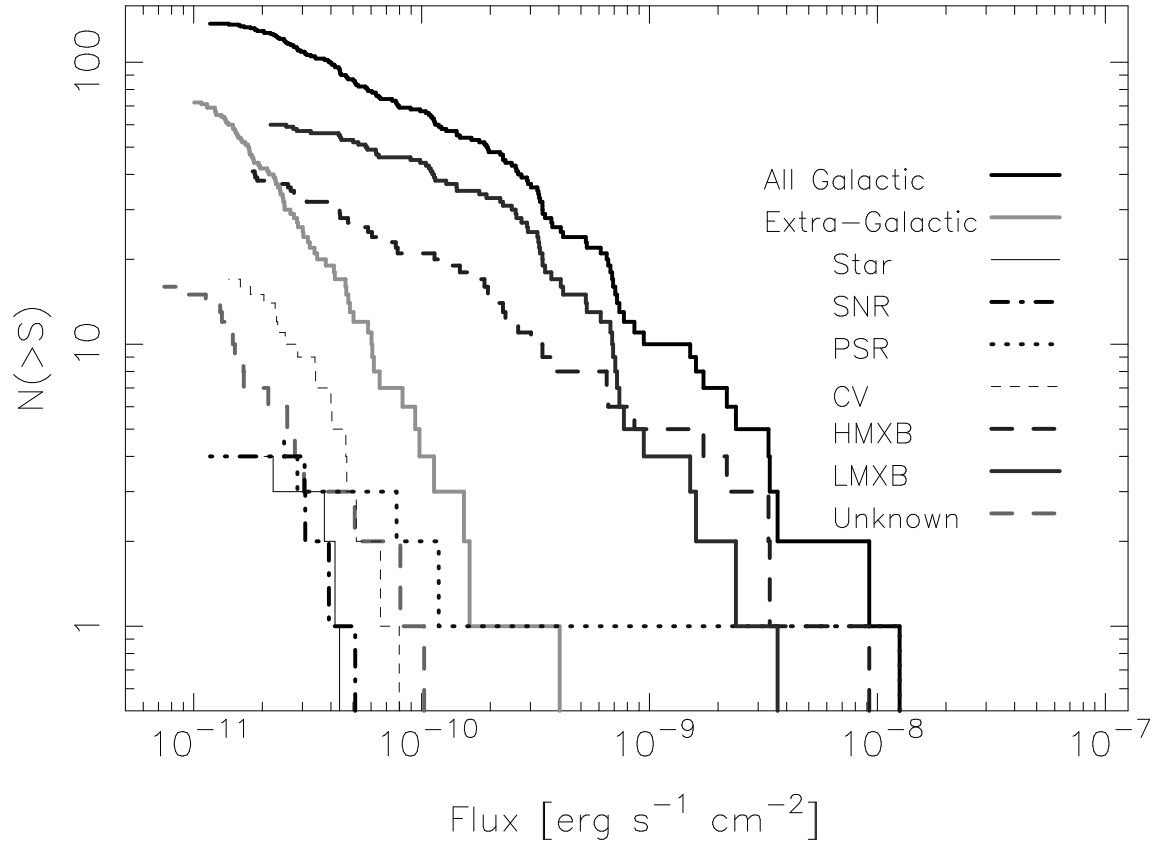


Fig. 10.— Cumulative logN-logS distributions of the observed sources.

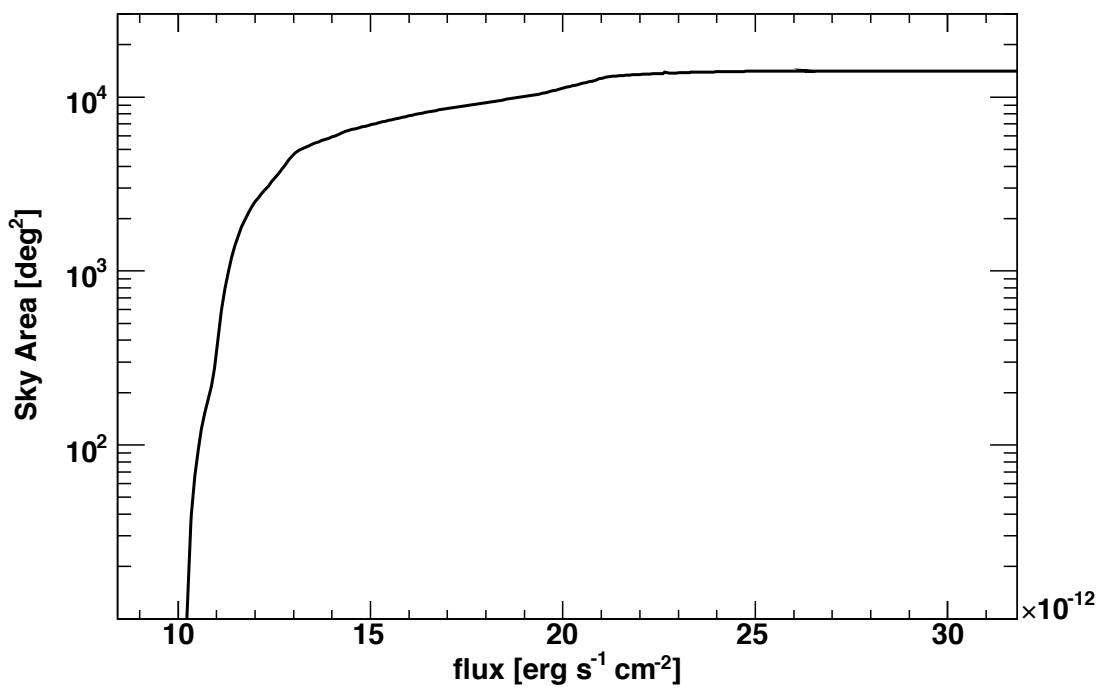


Fig. 11.— The sky coverage of the survey as a function of flux. The sensitivity depends on the local exposure and background, and is worse in the vicinity of bright sources. Above $\sim 2 \times 10^{-11} \text{ erg s}^{-1} \text{ cm}^{-2}$ the coverage quickly approaches a value of $\sim 14000 \text{ deg}^2$, corresponding to the full area within 20 deg of latitude from the Galactic plane.

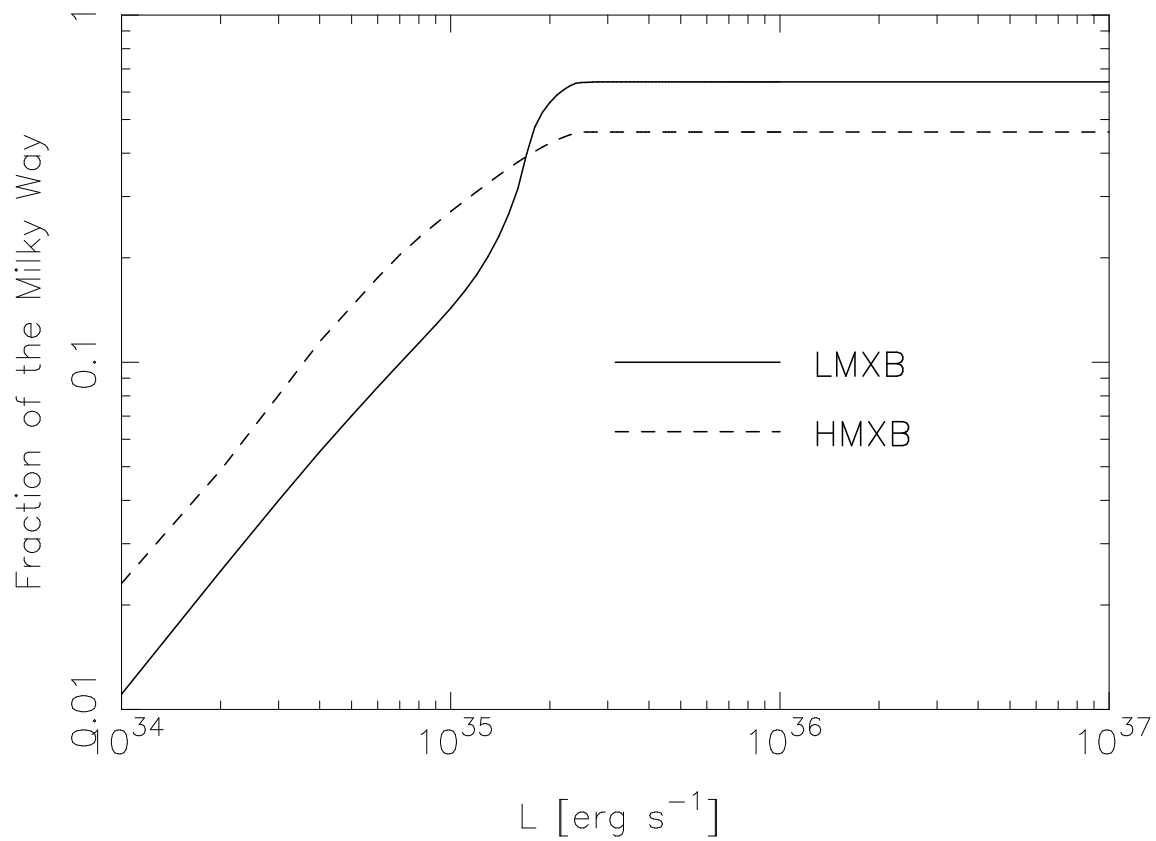


Fig. 12.— Fraction of the mass of the Galaxy probed by our survey, given the selection criteria described in the text.

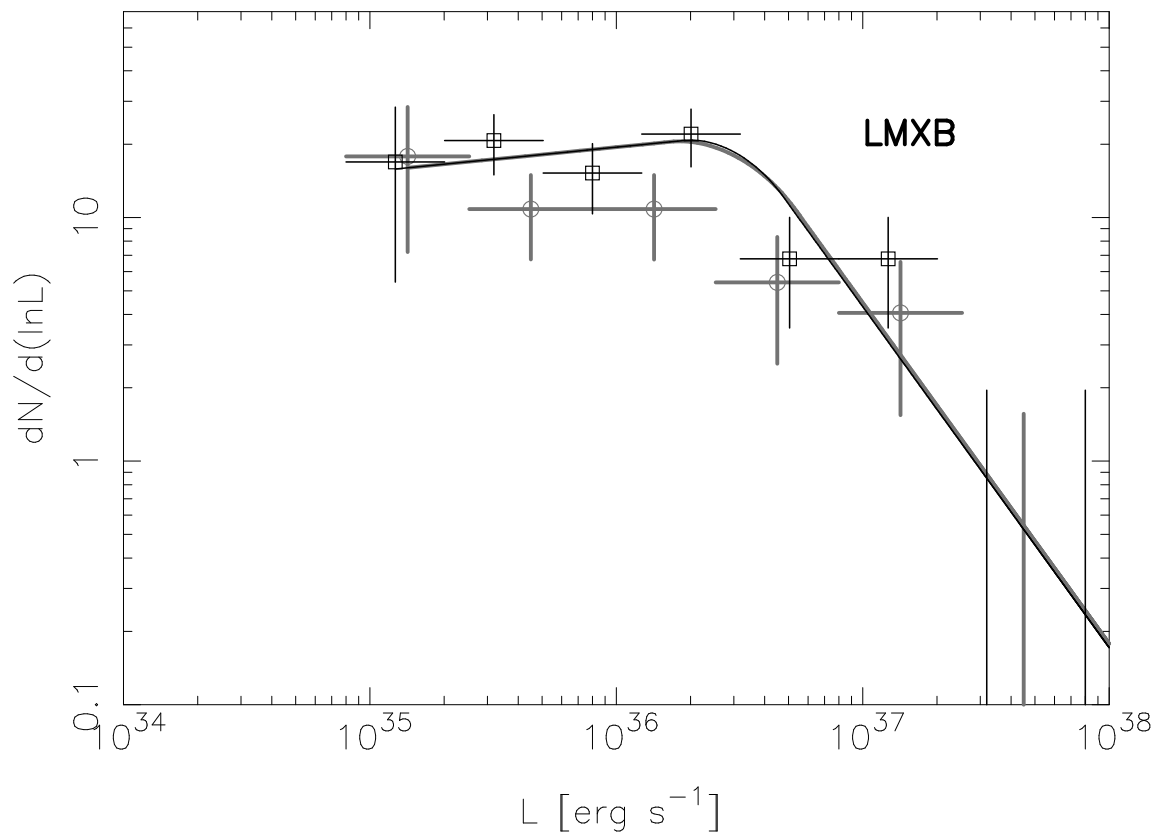


Fig. 13.— The luminosity function of Galactic LMXBs in the 15–55 keV band, corrected for incompleteness, with Poissonian errors. Squares indicate the results from the entire survey, whereas the inner 10 deg of the bulge were excluded for the circles. The solid black line shows the best maximum likelihood fit to the data from the entire survey, see Table 5.

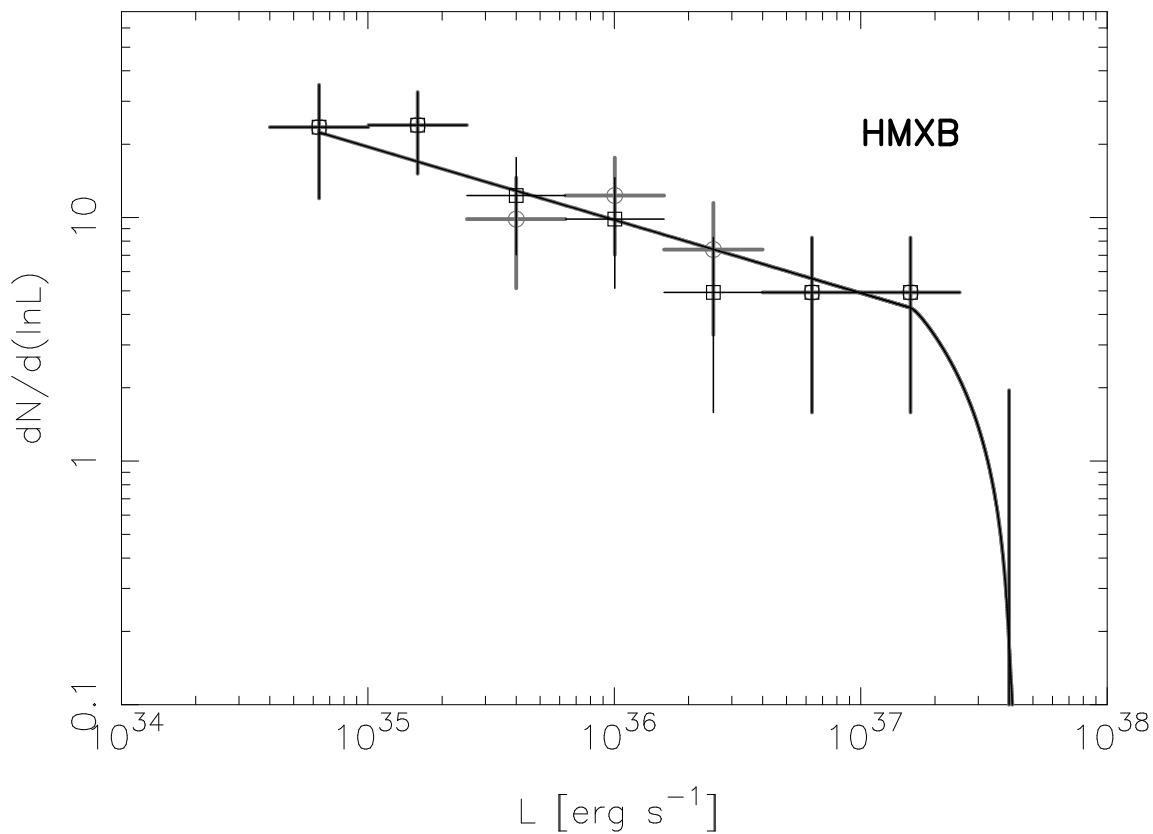


Fig. 14.— The luminosity function of Galactic HMXBs in the 15–55 keV band, corrected for incompleteness, with Poissonian errors. Squares indicate the results from the entire survey, whereas the inner 10 deg of the bulge were excluded for the circles. The solid black line shows the best maximum likelihood fit to the data from the entire survey, see Table 5.

REFERENCES

- Ajello, M., Greiner, J., Kanbach, G., Rau, A., Strong, A. W., & Kennea, J. A. 2008a, *ApJ*, 678, 102
- Ajello, M., et al. 2008b, *ApJ*, 689, 666
- . 2008c, *ApJ*, 673, 96
- . 2009, *ApJ*, 690, 367
- Almaini, O., et al. 2000, *MNRAS*, 315, 325
- Bahcall, J. N., & Soneira, R. M. 1980, *ApJS*, 44, 73
- Barcons, X., Franceschini, A., de Zotti, G., Danese, L., & Miyaji, T. 1995, *ApJ*, 455, 480
- Barthelmy, S. D., et al. 2005, *Space Science Reviews*, 120, 143
- Beckmann, V., Barthelmy, S. D., Courvoisier, T. J.-L., Gehrels, N., Soldi, S., Tueller, J., & Wendt, G. 2007, *A&A*, 475, 827
- Bird, A. J., et al. 2006, *ApJ*, 636, 765
- . 2007, *ApJS*, 170, 175
- Bogdán, Á., & Gilfanov, M. 2008, *MNRAS*, 388, 56
- Brinkmann, W., et al. 1997, *A&A*, 323, 739
- Brunschweiler, J., Greiner, J., Ajello, M., & Osborne, J. 2009, *A&A*, 496, 121
- Cole, S., et al. 2001, *MNRAS*, 326, 255
- Diehl, R., et al. 2006, *Nature*, 439, 45

- Flynn, C., Holmberg, J., Portinari, L., Fuchs, B., & Jahreiß, H. 2006, MNRAS, 372, 1149
- Gehrels, N., et al. 2004, ApJ, 611, 1005
- Georgelin, Y. M., & Georgelin, Y. P. 1976, A&A, 49, 57
- Gilfanov, M. 2004, MNRAS, 349, 146
- Gilfanov, M., Grimm, H.-J., & Sunyaev, R. 2004, MNRAS, 351, 1365
- Grimm, H.-J., Gilfanov, M., & Sunyaev, R. 2002, A&A, 391, 923
- . 2003, MNRAS, 339, 793
- Hanish, D. J., et al. 2006, ApJ, 649, 150
- Kaplan, D. L., Gaensler, B. M., Kulkarni, S. R., & Slane, P. O. 2006, ApJS, 163, 344
- Kim, D.-W., & Fabbiano, G. 2004, ApJ, 611, 846
- . 2010, ArXiv:astro-ph/1004.2427
- Kim, D.-W., et al. 2006, ApJ, 652, 1090
- . 2009, ApJ, 703, 829
- Krivosos, R., Revnivtsev, M., Lutovinov, A., Sazonov, S., Churazov, E., & Sunyaev, R.
2007, A&A, 475, 775
- Liu, Q. Z., van Paradijs, J., & van den Heuvel, E. P. J. 2005, A&A, 442, 1135
- . 2006, A&A, 455, 1165
- . 2007, A&A, 469, 807
- Lutovinov, A., Revnivtsev, M., Gilfanov, M., Shtykovskiy, P., Molkov, S., & Sunyaev, R.
2005, A&A, 444, 821

- Markwardt, C. B., Tueller, J., Skinner, G. K., Gehrels, N., Barthelmy, S. D., & Mushotzky, R. F. 2005, *ApJ*, 633, L77
- Mateos, S., Barcons, X., Carrera, F. J., Page, M. J., Ceballos, M. T., Hasinger, G., & Fabian, A. C. 2007, *A&A*, 473, 105
- Pietsch, W., Haberl, F., Sasaki, M., Gaetz, T. J., Plucinsky, P. P., Ghavamian, P., Long, K. S., & Pannuti, T. G. 2006, *ApJ*, 646, 420
- Ranalli, P., Comastri, A., & Setti, G. 2005, *A&A*, 440, 23
- Revnivtsev, M., Lutovinov, A., Churazov, E., Sazonov, S., Gilfanov, M., Grebenev, S., & Sunyaev, R. 2008, *A&A*, 491, 209
- Revnivtsev, M. G., et al. 2004, *Astronomy Letters*, 30, 382
- Salucci, P., & Persic, M. 1999, *MNRAS*, 309, 923
- Shtykovskiy, P., & Gilfanov, M. 2005, *A&A*, 431, 597
- Smith, D. M., Heindl, W. A., Markwardt, C. B., Swank, J. H., Negueruela, I., Harrison, T. E., & Huss, L. 2006, *ApJ*, 638, 974
- Taylor, J. H., & Cordes, J. M. 1993, *ApJ*, 411, 674
- Tueller, J., et al. 2010, *ApJS*, 186, 378
- Voges, W., et al. 1999, *A&A*, 349, 389
- Voss, R., & Gilfanov, M. 2006, *A&A*, 447, 71
- . 2007, *A&A*, 468, 49
- Voss, R., et al. 2009, *ApJ*, 701, 471

Walter, R., et al. 2006, *A&A*, 453, 133

Woodley, K. A., et al. 2008, *ApJ*, 682, 199

Zhang, S., Chen, Y., Wang, J., Torres, D. F., & Li, T. 2009, *A&A*, 502, 231

Table 1. The 228 detected hard X-ray sources ^a.

SWIFT NAME	R.A. (J2000)	Dec. (J2000)	σ (pos) (arcmin)	Flux (10^{-11} cgs)	S/N	ID	Type	Offset (arcmin)
J0018.8+8136	4.700	81.600	4.925	1.23	5.0	QSO J0017+8135	BLAZAR	3.7
J0024.9+6407	6.235	64.128	4.341	1.33	5.5	4U 0022+63	SNR	2.6
J0028.6+5918	7.162	59.301	2.063	6.11	25.0	V709 Cas	CV	1.4
J0035.7+5951	8.949	59.850	3.992	1.61	6.5	1ES 0033+59.5	BLLAC	1.1
J0055.2+4613	13.802	46.219	3.535	2.00	7.5	1RXS J005528.0+461143	CV	3.0
J0056.5+6042	14.127	60.705	2.544	7.11	28.6	Gam Cas	Be star	1.0
J0118.0+6517	19.503	65.293	0.948	15.45	64.3	4U 0114+65	HMXB	0.3
J0146.5+6144	26.635	61.745	3.158	2.49	9.7	PSR J0146+61	PSR	1.2
J0209.8+5227	32.453	52.453	3.727	2.75	9.9	SWIFT J0209.7+5226	Sy1	1.8
J0216.2+5126	34.051	51.449	4.090	1.69	6.0	SWIFT J0216.3+5128	Sy2	2.8

^aThe full table is available in the online version of the paper.

Table 2. Tentative ID for Unidentified Sources

SWIFT NAME	R.A. (J2000)	Decl. (J2000)	S/N	ID	Type	Offset (arcmin)
J0457.2+4527	74.301	45.452	5.2	1RXS J045707.4+452751	AGN ^a	1.1
J0746.1-1611	116.549	-16.199	7.2	1RXS J074616.8-161127		1.3
J0826.1-7030	126.531	-70.509	6.1	1ES 0826-70.3		1.7
J2056.6+4942	314.153	49.700	5.2	RX J2056.6+4940	AGN ^b	2.0

^aThe extragalactic nature of 1RXS J045707.4+452751 has been proposed by Kaplan et al. (2006) on the basis of the hard X-ray spectrum and the X-ray-to-IR flux ratio.

^bThe nature of RX J2056.6+4940 is likely extragalactic because of its association with a radio-loud object (Brinkmann et al. 1997).

Table 3. Numbers of different source types in our catalogue.

CLASS	Number
LMXB	61
HMXB	43
CV	19
Supernova remnant	6
Pulsar	6
Star: symbiotic	4
Star: Dwarf Nova	1
AGN: Seyfert	56
AGN: BL Lac	2
AGN: Blazar	7
AGN: undefined	5
Galaxy cluster	3

Table 4. Average spectral properties of Galactic sources derived from the analysis of stacked spectra.

CLASS	N. Objects	Photon index	kT ^a (keV)
LMXB($HR_2 > 0.6$)	21	$2.25^{+0.83}_{-0.82}$	$2.7^{+0.19}_{-0.25}$
LMXB($HR_2 < 0.6$)	38	$2.74^{+0.06}_{-0.05}$...
HMXB	38	2.44 ± 0.05	...
CV	18	...	$22.68^{+2.39}_{-2.08}$
SNR	5	$1.84^{+0.32}_{-0.41}$	$6.23^{+3.80}_{-2.67}$

^aBest-fit temperature for a black-body model (LMXBs) or a bremsstrahlung model (CVs/SNRs)

Table 5. Broken power-law fits to the LMXB and HMXB luminosity functions

Type	Lum. limit	Nr.	Faint slope	Break	Bright slope	Total lum. ^a	Total luminosity ^b
LMXBs	8×10^{34}	81.4 ± 15.0	$0.9^{+0.4}_{-0.3}$	$3.0^{+1.8}_{-1.6} \times 10^{36}$	$2.4^{+0.4}_{-0.7}$	$1.7 \pm 0.4 \times 10^{38}$	$1.5^{+1.5}_{-0.3} \times 10^{38}$
HMXBs	4×10^{34}	73.1 ± 15.4	$1.3^{+0.2}_{-0.2}$	$2.5^{+2.0}_{-2.3} \times 10^{37}$	> 2	$1.3 \pm 0.6 \times 10^{38}$	$1.4^{+1.5}_{-0.3} \times 10^{38}$

^aFrom summing individual source luminosities corrected for incompleteness.

^bFrom integrating the fitted luminosity function.